frontiers in Materials

ORIGINAL RESEARCH
published: 17 January 2022
doi: 10.3389/fmats.2021.818698

Mechanical Properties and Microstructure Evolution of Cemented Tailings Backfill Under Seepage Pressure

Yuxian Ke[1,2], *Yang Shen*[1,2], *Chen Qing*[3], *Kaijian Hu*[1,2]*, *Shi Wang*[1,2], *Qiusong Chen*[4]* and *Huadong Guan*[1]

[1]Jiangxi Province Key Laboratory of Mining Engineering, Jiangxi University of Science and Technology, Ganzhou, China, [2]School of Resources and Environment Engineering, Jiangxi University of Science and Technology, Ganzhou, China, [3]Periodical Press, Jiangxi University of Science and Technology, Ganzhou, China, [4]School of Resource and Safety Engineering, Central South University, Changsha, China

Cemented tailing backfill (CTB) in underground mine inevitably experiences seepage field, which complicates its mechanical behavior. In this study, the mechanical properties and microstructure characteristics of CTB under different seepage water pressures (SWPs) were investigated. The results show that, with the increase in SWP, the mechanical properties of CTB decrease, but the decreasing trend reduces gradually. Higher SWP leads the microstructure of CTB looser and more porous, and the largest proportion of pores initiated and propagated by SWP is micropores, which means the damage in CTB under seepage is mostly caused by micropores. Besides, the mechanical properties of CTB under seepage decrease exponentially with the increase in porosity and present linearly inverse proportional relation to the pore area fractal dimension. Results above indicate that SWP has a significant deterioration effect on the mechanical properties and microstructure of CTB. The research could not only extend the knowledge of mechanical properties and microstructure characteristics of CTB under seepage but also provide a theoretical reference for mechanical index determination and stability analysis of CTB in water-rich underground mines.

Keywords: cemented tailing backfill, paste backfill, mechanical properties, microstructure, seepage, green mining

OPEN ACCESS

Edited by:
Shuai Cao,
University of Science and Technology Beijing, China

Reviewed by:
Junmeng Li,
China University of Mining and Technology, China
Lang Liu,
Xi'an University of Science and Technology, China

***Correspondence:**
Kaijian Hu
hukaijian@jxust.edu.cn
Qiusong Chen
qiusong.chen@csu.edu.cn

Specialty section:
This article was submitted to Structural Materials, a section of the journal Frontiers in Materials

Received: *19 November 2021*
Accepted: *07 December 2021*
Published: *17 January 2022*

Citation:
Ke Y, Shen Y, Qing C, Hu K, Wang S, Chen Q and Guan H (2022) Mechanical Properties and Microstructure Evolution of Cemented Tailings Backfill Under Seepage Pressure. Front. Mater. 8:818698. doi: 10.3389/fmats.2021.818698

INTRODUCTION

Cemented tailing backfilling is the most effective way to maximize the utilization of tailings and to minimize the amounts of environmental hazards (Ke et al., 2017a; Cao et al., 2018; Li et al., 2021a; Li et al., 2021b; Tana et al., 2021). It has become the preferred mining method for the sustainable development of underground mining industry (Fall and Samb, 2009; Ke et al., 2017b; Yu et al., 2021; Chen et al., 2022). One of the global concerns in this means is the high cost of cemented tailing backfill (CTB) due to the high cement dosage. A decrease in cement dosage can significantly reduce the cost for the binder; cost takes up 60% to 80% of CTB total cost (Ghirian and Fall, 2013; Ghirian and Fall, 2014; Tan et al., 2019; Li et al., 2021d). However, the desired strength of CTB is mainly provided by the hydration of cement. Reducing the cement content will severely restrict the strength of CTB and cause potential security threats to mining operations (Yilmaz et al., 2015; Behera et al., 2021). Usually, the strength index of CTB is bound to be conservatively designed under safety first

situation, resulting in large cement consumption and high cost. The mechanical properties of CTB are the fundamental basis for determining its reasonable strength index (Xu et al., 2019; Qiu et al., 2020; Yin et al., 2020; Qi et al., 2021). Therefore, it is of great theoretical value and practical application significance to clearly understand the mechanical properties of CTB under different conditions.

At present, numerous researches have already been carried out to investigate the effect of various factors on the mechanical properties of CTB. Cao et al. (2018) concluded that uniaxial compressive strength (UCS) of CTB increases with the higher cement-tailings ratio and solid concentration. Xu et al. (2020) and Jiang et al. (2020) studied the influence of curing age on the mechanical properties of CTB, which concluded that the increase in curing age could remarkably improve the UCS of CTB. Fall et al. (2010), Wu et al. (2021), Chen et al. (2021a), Chen et al. (2021b), and Haiqiang et al. (2016) noted that curing temperature had a significant impact on the strength development of CTB, and the appropriate temperature conducive to improving the mechanical performance of CTB is approximately 50°C. Yilmaz et al. (2009) investigated the influence of curing pressure on mechanical properties of CTB by a self-designed test system and observed that the compressive strength development of CTB curing under vertical pressure was higher than that without vertical pressure ones, which could be mainly due to the applied pressure during curing process and improved consolidation process of the CTB material. Xiu et al. (2021) and Cao et al. (2019a) studied the effects of loading rates on the UCS of CTB and found that the increase in loading rate had a strengthening effect on the UCS, and the correlation between the UCS and the loading rates was more consistent with exponential function when the loading rates were between 0.1 and 2 mm/min. Wang et al. (2020a) reported that cyclic loading and unloading had perceptible effect on the mechanical properties of CTB, and the direct reason for the change of UCS is the change of deformation modulus caused by cyclic loading and unloading. In addition, to improve the mechanical properties of CTB, many scholars investigated the influence of alternative binders [fly ash (Behera et al., 2020), lime (Sharma and Kumar, 2021), limestone powder (Zheng et al., 2016), granulated blast furnace slag (Mashifana and Sithole, 2021), copper slag (Chen et al., 2021c), and lithium slag (He et al., 2019)], synthetic fibers [polypropylene fibers (Chakilam and Cui, 2020), polyacrylonitrile fibers (Cao et al., 2019b), and glass fibers (Zhou et al., 2021)], and plant fibers [rice straw (Wang et al., 2020b; Chen et al., 2020) and corn straw (Wang et al., 2021a)] on the mechanical properties of CTB. The above literatures obtained plentiful valuable results and enhanced the understanding of the mechanical properties of CTB. However, there is no relevant research that considered the influence of groundwater seepage on the mechanical properties of CTB. The groundwater is the most common fluid in mining, which is related to more than 60% of mine engineering damage. It is one of the most important factors affecting mine engineering safety, especially in water-rich underground mines. Many researches have been conducted to reveal the influence of water seepage on the mechanical properties of rock materials. Wang et al. (2015) found that there were obvious weakening effects of seepage pressures on the mechanical properties after coarse sandstone damages. Xiao et al. (2020) applied triaxial compressive test on red sandstone under seepage pressure and concluded that seepage pressure reduced the stress eigenvalues of rocks and affected its value of strain stiffness. Kou et al. (2021) reported that seepage pressure promotes tensile crack initiation and propagation of artificial rock-like materials, and its ultimate failure mode transforms from pure shear failure mode to the mixed tensile-shear one with the increase in seepage pressure. The CTB, a kind of artificial functional composite materials, is filled with a large number of micropores and microcracks. Groundwater can easily flow through these micropores form seepage, which would induce the initiation and propagation of defects such as micropores and microcracks in CTB, and result in the change of its mechanical properties.

This article aims to explore the effect of SWP on the mechanical properties and microstructure characteristics of CTB. The seepage experiments were applied to simulate the damage of CTB caused by different SWPs. The mechanical properties of CTB with different SWPs were evaluated by UCS test. Then, microstructure characteristics of CTB were analyzed using nuclear magnetic resonance (NMR) and scanning electron microscopy (SEM). Next, the relationships among mechanical properties (UCS and elastic modulus), microstructure characteristics (pore size distribution, porosity, and fractal dimension), and SWP were established. The research results can provide a theoretical and fundamental basis to determine the UCS and elastic modulus indexes and analyze the stability of CTB in water-rich underground mines.

MATERIALS AND METHODS

Experimental Materials

Tailings

The tailings used for preparing CTB specimens were derived from a copper mine in Jiangxi Province, China. The particle size distribution of the tailings was analyzed using a laser particle size analyzer (Winner 2000), as shown in **Figure 1**. The effective diameter d_{10}, median diameter d_{50}, and constrained diameter d_{60} were 5.62, 68.41, and 90.88 μm, respectively, indicating the particle size of the tailings was medium to fine. The nonuniformity coefficient C_u and curvature coefficient C_c of the particles were 16.17 and 2.15, respectively, indicating a wide size distribution and a well particle gradation continuity of tailings. Furthermore, the main chemical compositions of the tailings were determined via X-ray fluorescence spectroscopy (XRF-1800), and the details of main chemical compositions of the tailings are shown in **Table 1**. The proportions of SiO_2 and CaO in the tailings were 33.02% and 15.68%, respectively, which is benefit to the strength development of CTB.

Binder and Water

The binder used in the preparation of CTB specimens was ordinary Portland cement (P.O32.5), commonly used in the copper mine. The chemical compositions of the P.O32.5 are listed in **Table 2**, and the specific gravity and specific surface

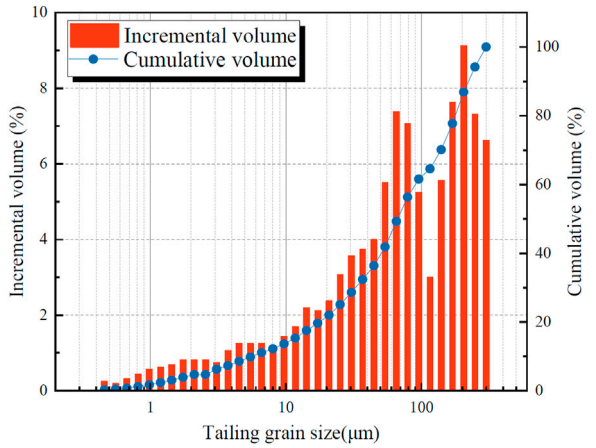

FIGURE 1 | Particle size distribution of tailings.

area of the P.O32.5 are 3.15 and 1.1 m^2/g, respectively. The mixed water was common tap water.

Experimental Methods

The experimental procedure is shown in **Figure 2**, which consisted of CTB specimen preparation, seepage experiment, NMR test, UCS test, and SEM test.

CTB Specimen Preparation

Three CTB specimens were prepared for each experimental condition, and the average results of each experimental condition are shown for further analysis. Cylindrical molds with a diameter of 50 mm and a height of 100 mm were used to make the CTB specimens, and the backfill pulp was mixed with the cement–tailing mass ratio of 1:4 and the solid mass concentration of 76% according to backfilling practice in the copper mine. Then, uniformly stirred pulp was poured into the

TABLE 1 | Chemical composition of the tailings.

Composition	SiO_2	CaO	Fe	S	Al_2O_3	MgO	K	Mn	F	Cu	P	Pb
wt%	33.02	15.68	10.37	4.55	2.56	1.82	0.37	0.085	0.080	0.065	0.049	0.0095

TABLE 2 | The chemical composition of P.O32.5.

Compositions	CaO	SiO_2	Al_2O_3	Fe_2O_3	SO_2	MgO	Na_2O	Other
wt%	63.66	21.26	4.5	2.8	2.58	1.66	0.18	3.36

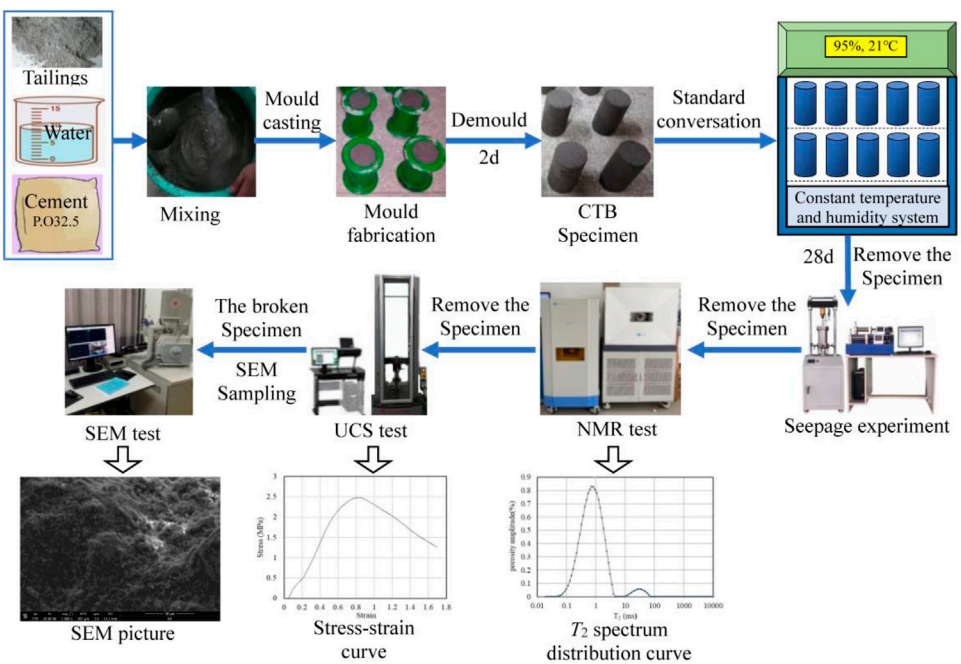

FIGURE 2 | Schematic diagram of experiments routine.

cylindrical molds and gently vibrated the sample holders a few times to eliminate bubbles. The CTB specimens were taken out of the molds after 2 days and cured in a constant temperature and humidity standard curing box (temperature of 20°C ± 1°C, humidity of 90%) for 28 days. Finally, the diameter and height of the cured CTB specimen were measured and recorded before the experiments.

Seepage Experiment

In this study, the seepage experiments were carried out on KSR-100 backfill triaxial creep test system (Jiangsu Yongchang Instrument Corporation, Suzhou, China). The KSR-100 owns three independent control systems for axial pressure, confining pressure, and seepage pressure, with the maximum axial load, confining pressure and seepage pressure being 100 kN, 10 MPa, and 10 MPa, respectively. Usually, the height of mining stope is less than 100 m, and there is a gap between the CTB and roof; the SWP in CTB is less than 1.0 MPa during mining operation. Thus, the SWPs were set to 0, 0.2, 0.5, and 0.8 MPa in the experiment, and the confining pressure kept constant at 1.0 MPa as it should be limited to be greater than the maximum SWP. Besides, the seepage water was tap water and has a pH of 7.0. The specific experimental scheme is shown in **Table 3**.

The stress state of CTB specimen during seepage experiment is presented in **Figure 3**. The seepage experiment steps are as follows: (1) placing porous discs at both ends of CTB specimen and wrap them (except at both ends) with a layer of heat-shrink film and installing them on the base of the KSR-100; (2) simultaneously applying confining pressure and axial pressure to 1.0 MPa at a loading rate of 2 kPa/min; (3) applying seepage pressure to predetermined value at the same loading rate when confining pressure and axial pressure were stable and kept for a period of time (approximately 72 h according to the experiment results) until the water seepage volume-time curve changed steadily; (4) unloading seepage pressure and simultaneously unloading confining pressure and axial pressure at the same unloading rate of 2 kPa/min; and (5) terminating the seepage experiment and taking out the sample for subsequent experiments.

NMR Test

The heat-shrink film was removed from the CTB specimens after seepage experiment, and the excess moisture was wiped off from the surface of CTB specimens. Then, the CTB specimens were fully wrapped with a layer of polytetrafluoroethylene film to avoid moisture loss before the NMR test. An NM-60 NMR instrument (Suzhou Niumag Analytical Instrument Corporation, Suzhou, China) was applied to perform the NMR test on CTB specimens, and the distribution of transverse relaxation time (T2) of CTB specimens can be obtained. The NMR test detail parameters refer to literatures (Gao et al., 2020; Hu et al., 2020; Wang et al., 2021b).

UCS Test

After the NMR test, the CTB specimens were removed to an electronic universal testing machine (WDW-20H; Jinan Huaxing Instrument Corporation, Jinan, China) for UCS test. The loading speed was 0.5 mm/min. Then the stress–strain curve, UCS, and elastic modulus of CTB specimens can be obtained.

SEM Test and Image Preprocessing

Once the UCS test was accomplished, one cubic sample with a side length of approximately 1 cm was cut from the center part of the broken CTB specimen for SEM test. An SEM system (MLA650F, USA) was applied to observe the microstructure of the CTB specimens, and more than 10 SEM images for each CTB

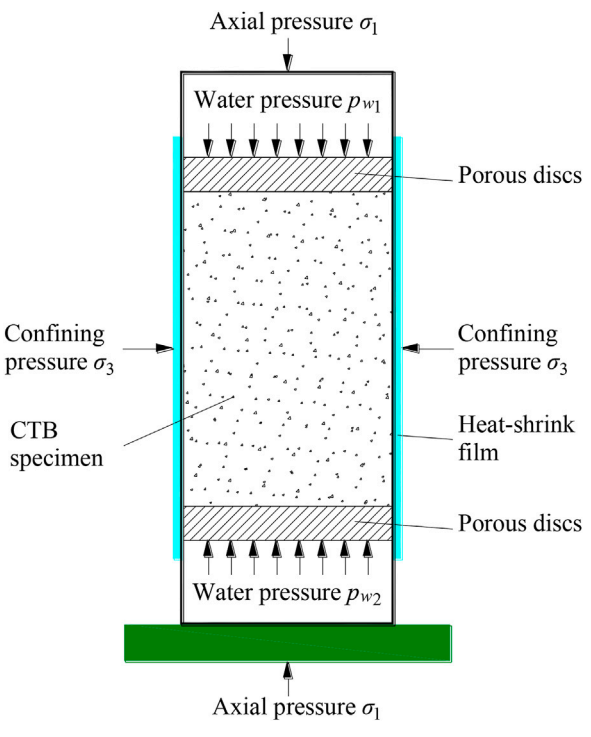

FIGURE 3 | Schematic diagram of stress of CTB specimen during seepage experiment.

TABLE 3 | Seepage experiment scheme.

Specimen number	Cement/tailings	Concentration (wt.%)	SWP (MPa)	Confining pressure (MPa)
ST-1, ST-2, ST-3	1:4	76	0	1.0
ST-4, ST-5, ST-6			0.2	
ST-7, ST-8, ST-9			0.5	
ST-10, ST-11, ST-12			0.8	

specimen were obtained. Prior to the test, the cubic sample was dried at 50°C and sprayed with gold.

It is generally accepted that the SEM micrograph is difficult to be directly used for quantitative analysis, although in this article the SEM micrograph was binary-processed using the MATLAB image processing toolbox and the obtained binary SEM micrograph was a black-and-white bitmap, in which the black and white regions represent the pore and structure, respectively. Correspondingly, for each experimental condition, nine SEM micrographs were preprocessed, and their mean results were used for further quantitative analysis.

RESULTS AND DISCUSSION

Effect of Seepage on Mechanical Properties of CTB

The UCS and elastic modulus are the two most important mechanical property parameters of CTB. Therefore, the UCS and elastic modulus of CTB under different SWPs were obtained for analysis. As shown in **Figure 4**, with an increase in SWP from 0 to 0.8 MPa, the UCS of CTB specimens decreased from 6.11 to 4.08 MPa; the elastic modulus decreased from 7.27×10^2 to 4.14×10^2 MPa. The UCS loss rates of CTB specimens were 17.18%, 28.97%, and 33.22%, and the elastic modulus loss rates of CTB specimens were 24.07%, 37.14%, and 43.05% when the SWP increased from 0 to 0.2 MPa and, 0.5 and 0.8 MPa, respectively. The results suggested that SWP had an obvious weakening effect on the UCS and elastic modulus of CTB, whereas the weakening effect was decreasing overall with the increase in SWP; that is, the higher the SWP, the less apparent the weakening effect on mechanical properties of CTB. The weakening effect of SWP on the UCS and elastic modulus are consistent with the findings reported by Hou et al. (2020). In addition, the mechanical properties of CTB are related to its internal microstructure (Yang et al., 2019; Zhou et al., 2019; Tana et al., 2021); the results indicated that the seepage would cause a certain degree of damage to the internal microstructure of CTB.

Microstructure Characteristics of CTB Under Different SWPs

Effect of SWP on Porosity of CTB

The porosity is a key feature reflecting the variation in microstructure characteristics of CTB. The porosity of CTB specimens under different SWPs was obtained from NMR test results, as shown in **Figure 5**. It can be noted that the porosity increased obviously with the increase in SWP. With an increase in SWP from 0 to 0.8 MPa, the porosity of CTB specimens increased from 4.687% to 15.337%. The porosity of CTB specimens increased by 3.390, 7.699, and 10.650 when the SWP increased from 0 to 0.2 MPa, 0.5 and 0.8 MPa, respectively. The results proved that SWP had a significant promoting effect on the initiation and propagation of pores and microcracks in CTB specimens, which contributed to the porosity and microstructure damage of CTB specimens. Meanwhile, a high SWP corresponded to a higher promoting effect, whereas the influence rate was gradually decreasing.

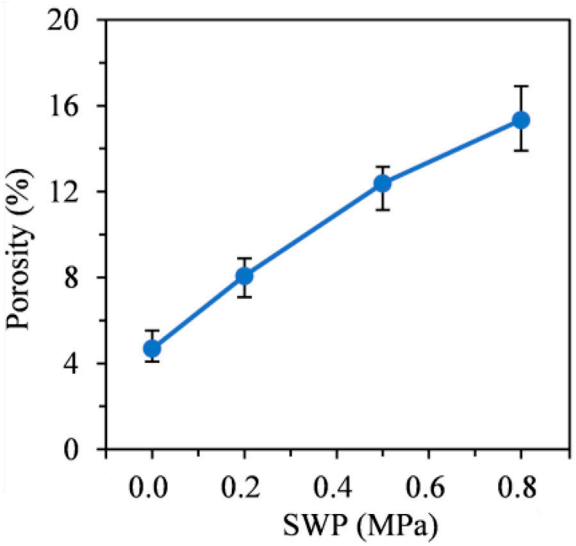

FIGURE 5 | Effect of seepage on porosity of CTB specimens.

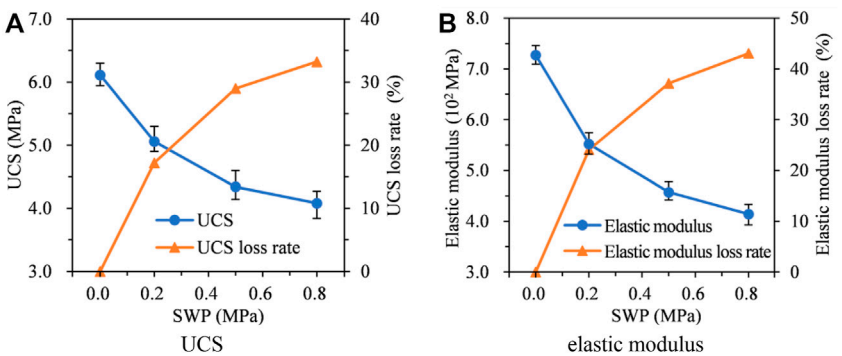

FIGURE 4 | Effect of seepage on **(A)** UCS and **(B)** elastic modulus of CTB specimens.

Effect of Seepage on Pore Size Distribution Characteristics of CTB

According to the NMR measurement principle, a smaller T_2 value represents a smaller pore size, and *vice versa*. **Figure 6** shows the T_2 distribution of CTB specimens after adopting a different SWPs. It can be found that there were three peaks at each T_2 distribution. Peak 1 (leftmost peak) was obviously higher than peak 2 (middle peak), and peak 2 was obviously higher than peak 3 (rightmost peak), indicating that most of the main pores of CTB specimens were micropores, followed by mesopores, and the least were macropores. The three peaks were discontinuous, revealing that there was no direct link channel among the three kinds of pores. **Figure 7** shows the variation law of peak area of CTB specimens with SWP. As can be seen, with the increase in SWP; peaks 1 and 2 areas of CTB specimens showed an obvious increasing trend, whereas peak 3 area hardly changed. With an increase in SWP from 0 to 0.8 MPa, peak 1 area increased from 4.492 to 14.841, and peak 2 area increased from 0.132 to 0.439, and the areas of peaks 1 and 2 accounted for 98.67% to 99.63% of the total peak area. Peak 1 area increased by 3.258, 7.508, and 10.349; and peak 2 area increased by 0.131, 0.202, and 0.307 when the SWP increased from 0 to 0.2 MPa, 0.5 and 0.8 MPa, respectively. The results suggested that the pores in CTB specimens initiated and propagated by seepage were mainly micropores and mesopores, and the macropore volume hardly affected by SWP. To sum up, micropore volume of CTB was the most increasing one as SWP increased, and the damage in CTB under seepage was mostly caused by micropores.

Effect of SWP on Pore Area Fractal Dimension of CTB

Figure 8 shows the SEM micrographs and their binarization results of CTB specimens under different SWPs. With a larger SWP, the microscopic surface of specimen was looser, and the pore area was larger. The fractal dimension is one of the most important basic parameters of microstructure characteristics of CTB. Thus, fractal theory was used to analyze the effect of SWP on the pore area fractal dimension of CTB specimens in this study. The pore area fractal dimension of binarized SEM micrographs was determined via box counting (Zhao et al., 2022; Zhang et al., 2020; Wu et al., 2019; Sun et al., 2019). As shown in **Figure 9**, the changing regularity of SWP on pore area fractal dimension of CTB specimens was similar to SWP on porosity. With an increase in SWP from 0 to 0.8 MPa, the pore area fractal dimension of CTB specimens increased from 1.815 to 1.903. The pore area fractal dimension of CTB specimens increased by 0.036, 0.067, and 0.088 when the SWP increased from 0 to 0.2 MPa, 0.5 and 0.8 MPa, respectively. A large pore area fractal dimension represents a high complexity of pores and a worse uniformity of pores. These findings further indicated that a higher SWP will make the microstructure of CTB looser and more porous, resulting in more microcracks and pores. Microcracks propagated and connected with pores, forming defects, which deteriorated the microstructure and weakened the mechanical properties of CTB (Mower and Long, 2016; Gu et al., 2020).

Relationship Between Mechanical Properties and Microstructure Characteristics

Relationship Among UCS, Elastic Modulus, and Porosity

The porosity of CTB has an important influence on its mechanical properties. **Figure 10** shows the relationship

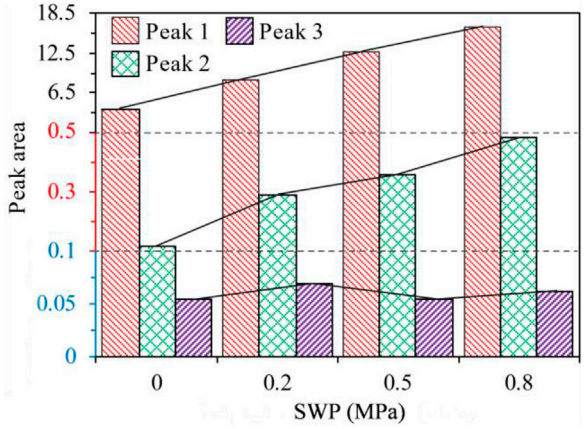

FIGURE 7 | Effect of SWP on peak area of CTB specimens.

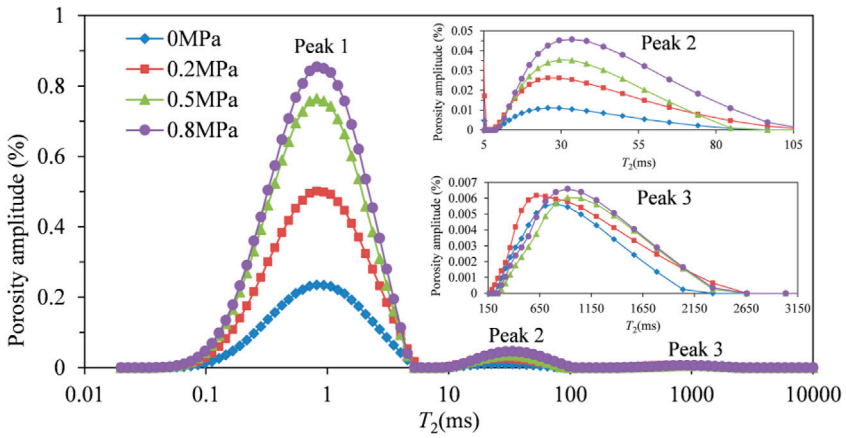

FIGURE 6 | Effect of SWP on T_2 distribution of CTB specimens.

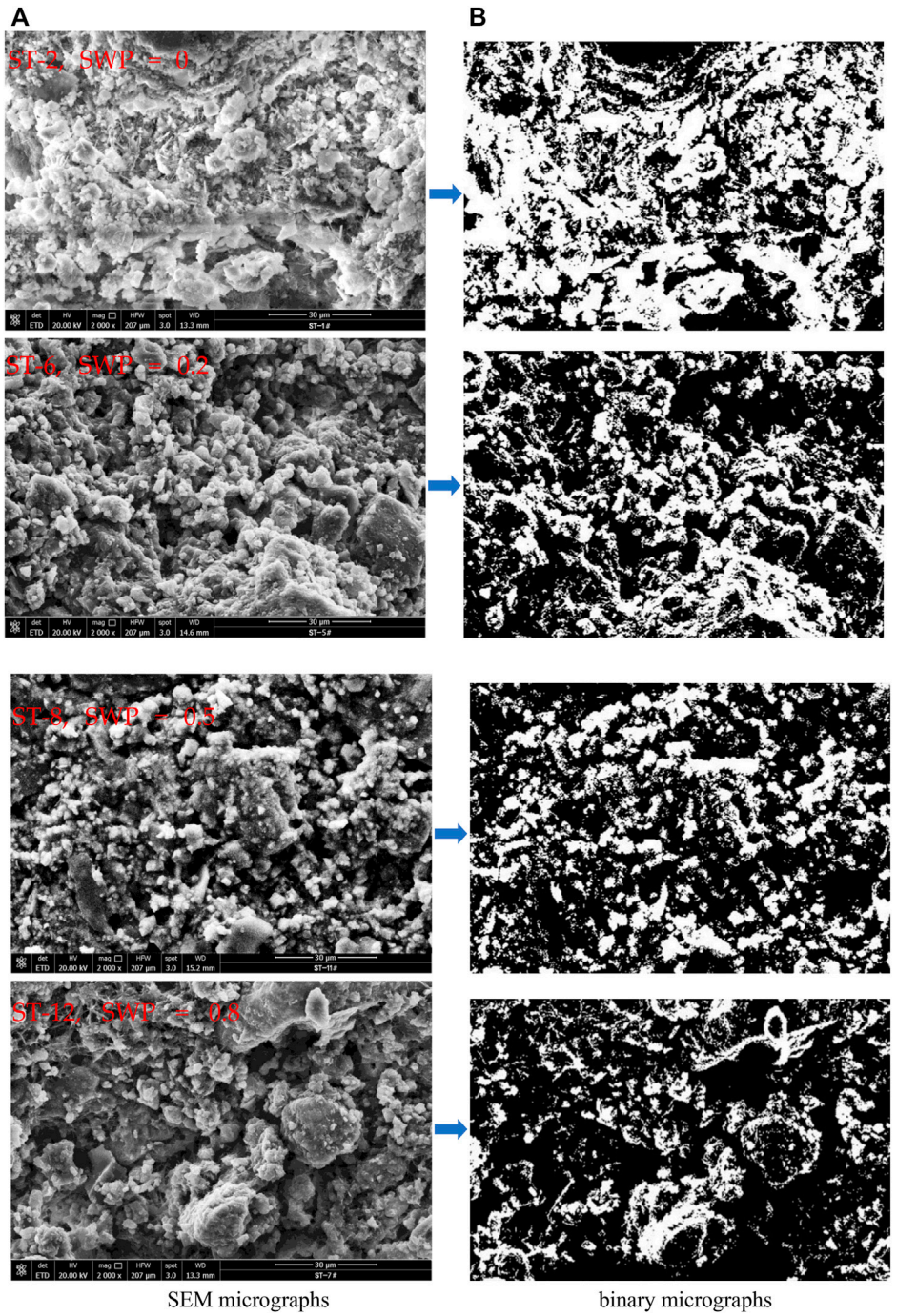

FIGURE 8 | (A) SEM micrographs and **(B)** binary micrographs of CTB specimens.

among UCS, elastic modulus, and porosity. It can be clearly seen that both the UCS and elastic modulus of CTB decreased with the increase in porosity, and both relationships were strongly nonlinear. The relationship among UCS, elastic modulus, and porosity can be fitted as $\sigma_c = 5.012e^{\frac{-n}{7.484}} + 3.393$ ($R^2 = 0.9529$) and $E = 7.896e^{\frac{-n}{6.168}} + 3.475$ ($R^2 = 0.9487$), respectively, where σ_c is the fitted UCS of CTB (MPa), E is the fitted elastic modulus of CTB (10^2 MPa), n is the porosity of CTB, and R is correlation coefficient. Both correlation coefficients were greater than 0.9, which demonstrated that the fitted equations were highly reliable. Thus, the UCS and elastic modulus of CTB under different

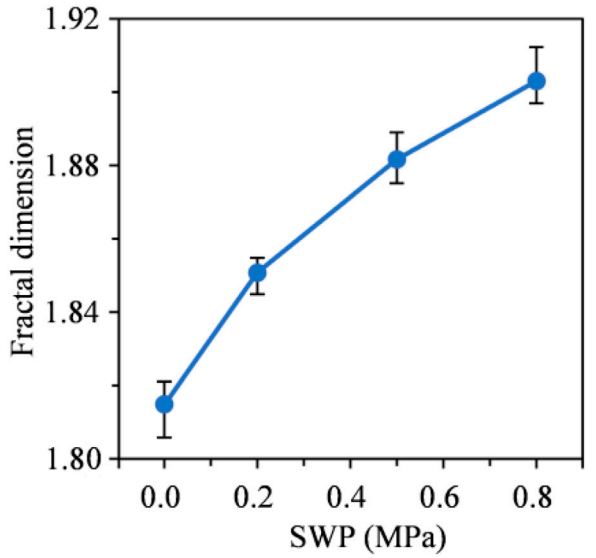

FIGURE 9 | Effect of SWP on pore area fractal dimension of CTB specimens.

SWPs can be evaluated using the above two fitting functions according to the porosity measured by NMR, which provides an effective method for obtaining UCS and elastic modulus of CTB under different SWPs.

Relationship Among UCS, Elastic Modulus, and Pore Area Fractal Dimension

The relationships among UCS, elastic modulus, and pore area fractal dimension for CTB are shown in **Figure 11**. It can be clearly seen that both the UCS and elastic modulus of CTB were negatively correlated with its pore area fractal dimension; that is, the higher the pore area fractal dimension, the lower the UCS and elastic modulus of CTB. The fitted line among UCS, elastic modulus, and pore area fractal dimension for CTB were $\sigma_c = -23.66D + 48.49$ $(R^2 = 0.9414)$, $E = -35.35D + 71.22$ $(R^2 = 0.9367)$, respectively, where D is the pore area fractal dimension of CTB. The two high correlation coefficients meant significant correlations and reliable fitting lines. These results indicated that the complexity of pores would lead to a lower UCS and elastic modulus of CTB, which was consistent with the findings by Ouellet et al. (2007) and Liu et al. (2020).

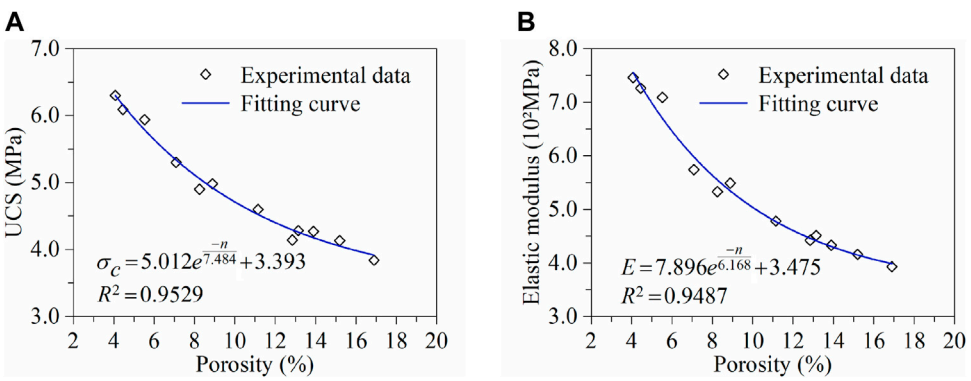

FIGURE 10 | Relationship among **(A)** UCS, **(B)** elastic modulus and porosity.

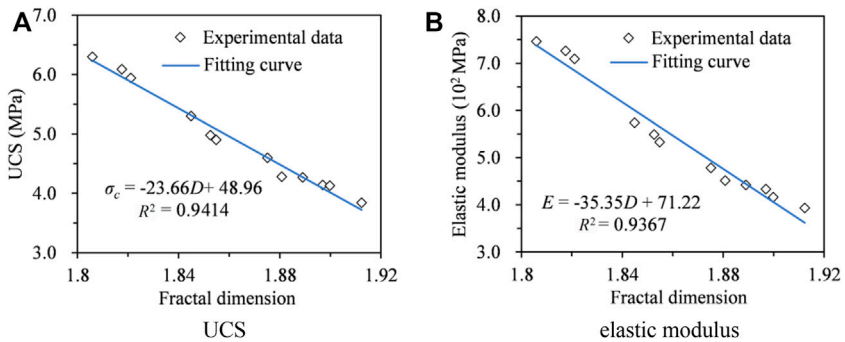

FIGURE 11 | Relationship among **(A)** UCS, **(B)** elastic modulus and pore area fractal dimension.

CONCLUSION

In this study, the effects of SWP on the mechanical properties and microstructure characteristics of CTB were studied through a series of laboratory experiments as follows: seepage experiments were conducted to simulate the damage of CTB caused by seepage; UCS tests were performed to obtain the mechanical properties of CTB. Also, NMR and SEM tests were used to analyze the microstructure characteristics of CTB. Based on the results presented in this article, the following conclusions can be drawn:

(1) Seepage had a significant deterioration effect on the mechanical properties of CTB. The UCS and elastic modulus of CTB decreased with the increase in SWP, whereas the decreasing trend reduced gradually with the increase in SWP.
(2) Seepage promoted the initiation and propagation of microcracks and pores in CTB. Higher SWP initiated and propagated more microcracks and pores in CTB, resulting in a looser and more porous microstructure of CTB, and a higher porosity and pore area fractal dimension, which seriously damaged the microstructure and weakened the mechanical properties of CTB.
(3) The T_2 spectrum showed that the pores in CTB with the largest proportion initiated and propagated by seepage were micropores, which means the damage in CTB under seepage mostly caused by micropores.
(4) The UCS and elastic modulus of CTB under seepage decrease exponentially with the increased porosity and present linearly inverse proportional relation to the pore area fractal dimension.

DATA AVAILABILITY STATEMENT

The original contributions presented in the study are included in the article/supplementary material, further inquiries can be directed to the corresponding authors.

AUTHOR CONTRIBUTIONS

Conceptualization, YK and YS; methodology, YK and KH; software, CQ, QC; validation, YS, CQ, and QC; formal analysis, YK, KH, and YS; investigation, YK, and CQ; resources, YS, and CQ; data curation, YK; writing—original draft preparation, YK and YS; writing—review and editing, KH, YK, YS, SW, QC, and HG; visualization, YK and CQ; supervision, YK, SW, KH, and HG; project administration, YS; funding acquisition, YK, SW, KH, and HG; All authors have read and agreed to the published version of the manuscript.

FUNDING

The research was supported by the National Natural Science Foundation of China (No. 51804135, 51804134), Natural Science Foundation of Jiangxi Province (No. 20192BAB216017), Doctoral Startup Fund of Jiangxi University of Science and Technology (No. jxxjbs17070), Program of Qingjiang Excellent Young Talents, Jiangxi University of Science and Technology (No. jxustqjyx2020007)and Science and technology research project of Jiangxi Provincial Department of Education (GJJ190499).

REFERENCES

Behera, S. K., Mishra, D. P., Singh, P., Mishra, K., Mandal, S. K., Ghosh, C. N., et al. (2021). Utilization of Mill Tailings, Fly Ash and Slag as Mine Paste Backfill Material: Review and Future Perspective. *Construction Building Mater.* 309, 125120. doi:10.1016/j.conbuildmat.2021.125120,

Behera, S. K., Ghosh, C. N., Mishra, D. P., Singh, P., Mishra, K., Buragohain, J., et al. (2020). Strength Development and Microstructural Investigation of lead-zinc Mill Tailings Based Paste Backfill with Fly Ash as Alternative Binder. *Cement Concrete Comp.* 109, 103553. doi:10.1016/j.cemconcomp.2020.103553

Cao, S., Yilmaz, E., and Song, W. D. (2018). Evaluation of Viscosity, Strength and Microstructural Properties of Cemented Tailings Backfill. *Minerals* 8, 352. doi:10.3390/min8080352

Cao, S., Yilmaz, E., and Song, W. (2019). Fiber Type Effect on Strength, Toughness and Microstructure of Early Age Cemented Tailings Backfill. *Construction Building Mater.* 223, 44–54. doi:10.1016/j.conbuildmat.2019.06.221

Cao, S., Yilmaz, E., Song, W., Yilmaz, E., and Xue, G. (2019). Loading Rate Effect on Uniaxial Compressive Strength Behavior and Acoustic Emission Properties of Cemented Tailings Backfill. *Construction Building Mater.* 213, 313–324. doi:10.1016/j.conbuildmat.2019.04.082

Chakilam, S., and Cui, L. (2020). Effect of Polypropylene Fiber Content and Fiber Length on the Saturated Hydraulic Conductivity of Hydrating Cemented Paste Backfill. *Construction Building Mater.* 262, 120854. doi:10.1016/j.conbuildmat.2020.120854

Chen, Q. S., Tao, Y. B., Feng, Y., Zhang, Q. L., and Liu, Y. K. (2021). Utilization of Modified Copper Slag Activated by Na2SO4 and CaO for Unclassified lead/zinc Mine Tailings Based Cemented Paste Backfill. *J. Environ. Manage.* 290, 112608. doi:10.1016/j.jenvman.2021.112608

Chen, Q., Tao, Y., Zhang, Q., and Qi, C. (2022). The Rheological, Mechanical and Heavy Metal Leaching Properties of Cemented Paste Backfill under the Influence of Anionic Polyacrylamide. *Chemosphere* 286, 131630. doi:10.1016/j.chemosphere.2021.131630

Chen, S. M., Wu, A. X., Wang, Y. M., and Wang, W. (2021). Correlation of Coupled Effects of Curing Stress and Curing Temperature on the Mechanical and Physical Properties of Cemented Paste Backfill Based on gray Relational Analysis. *Arab J. Geosci.* 14, 479. doi:10.1007/s12517-021-06659-6

Chen, S. M., Wu, A. X., Wang, Y. M., and Wang, W. (2021). Coupled Effects of Curing Stress and Curing Temperature on Mechanical and Physical Properties of Cemented Paste Backfill. *Construction Building Mater.* 273, 121746. doi:10.1016/j.conbuildmat.2020.121746

Chen, X., Shi, X. Z., Zhou, J., Yu, Z., and Huang, P. S. (2020). Determination of Mechanical, Flowability, and Microstructural Properties of Cemented Tailings Backfill Containing rice Straw. *Construction Building Mater.* 246, 118520. doi:10.1016/j.conbuildmat.2020.118520

Fall, M., Célestin, J. C., Pokharel, M., and Touré, M. (2010). A Contribution to Understanding the Effects of Curing Temperature on the Mechanical Properties of Mine Cemented Tailings Backfill. *Eng. Geology.* 114, 397–413. doi:10.1016/j.enggeo.2010.05.016

Fall, M., and Samb, S. S. (2009). Effect of High Temperature on Strength and Microstructural Properties of Cemented Paste Backfill. *Fire Saf. J.* 44, 642–651. doi:10.1016/j.firesaf.2008.12.004

Gao, R. G., Zhou, K. P., Liu, W., and Ren, Q. F. (2020). Correlation between the Pore Structure and Water Retention of Cemented Paste Backfill Using Centrifugal and Nuclear Magnetic Resonance Methods. *Minerals* 10, 610. doi:10.3390/min10070610

Ghirian, A., and Fall, M. (2014). Coupled Thermo-Hydro-Mechanical-Chemical Behaviour of Cemented Paste Backfill in Column Experiments. *Eng. Geology.* 170, 11–23. doi:10.1016/j.enggeo.2013.12.004

Ghirian, A., and Fall, M. (2013). Coupled Thermo-Hydro-Mechanical-Chemical Behaviour of Cemented Paste Backfill in Column Experiments. Part I: Physical, Hydraulic and thermal Processes and Characteristics. *Eng. Geology.* 164, 195–207. doi:10.1016/j.enggeo.2013.01.015

Gu, J. L., Yang, S. L., Gao, M. J., Bai, J., and Liu, K. (2020). Influence of Deposition Strategy of Structural Interface on Microstructures and Mechanical Properties of Additively Manufactured Al alloy. *Addit Manuf* 34, 101370. doi:10.1016/j.addma.2020.101370

Haiqiang, J., Fall, M., and Cui, L. (2016). Yield Stress of Cemented Paste Backfill in Sub-zero Environments: Experimental Results. *Minerals Eng.* 92, 141–150. doi:10.1016/j.mineng.2016.03.014

He, Y., Chen, Q., Qi, C., Zhang, Q., and Xiao, C. (2019). Lithium Slag and Fly Ash-Based Binder for Cemented fine Tailings Backfill. *J. Environ. Manage.* 248, 109282. doi:10.1016/j.jenvman.2019.109282

Hou, J., Guo, Z., Liu, W., and Zhang, Y. (2020). Mechanical Properties and Meso-Structure Response of Cemented Gangue-Fly Ash Backfill with Cracks under Seepage- Stress Coupling. *Construction Building Mater.* 250, 118863. doi:10.1016/j.conbuildmat.2020.118863

Hu, J.-h., Ren, Q.-f., Yang, D.-j., Ma, S.-w., Shang, J.-l., Ding, X.-t., et al. (2020). Cross-scale Characteristics of Backfill Material Using NMR and Fractal Theory. *Trans. Nonferrous Met. Soc. China* 30, 1347–1363. doi:10.1016/S1003-6326(20)65301-8

Jiang, F.-f., Zhou, H., Sheng, J., Kou, Y.-y., and Li, X.-d. (2020). Effects of Temperature and Age on Physico-Mechanical Properties of Cemented Gravel Sand Backfills. *J. Cent. South. Univ.* 27, 2999–3012. doi:10.1007/s11771-020-4524-6

Ke, Y., Wang, X., and Zhang, Q. (2017). Flocculating Sedimentation Characteristic of Pre-magnetized Crude Tailings Slurry. *Chin. J. Nonferrous Met.* 27, 392–398. doi:10.19476/j.ysxb.1004.0609.2017.02.021

Ke, Y., Wang, X., Zhang, Q., and Liu, E. (2017). Strength Determination of Crude Tailings Backfill in Deep Mine Based on Non-linear Constitutive Mode. *J. Northeast. University(Nat. Science)* 38, 280–283. doi:10.3969/j.issn.1005-3026.2017.02.026

Kou, M. M., Liu, X. R., Wang, Z. Q., and Tang, S. D. (2021). Laboratory Investigations on Failure, Energy and Permeability Evolution of Fissured Rock-like Materials under Seepage Pressures. *Eng. Fract Mech.* 247, 107694. doi:10.1016/j.engfracmech.2021.107694

Li, J., Cao, S., Yilmaz, E., and Liu, Y. P. (2021). Compressive Fatigue Behavior and Failure Evolution of Additive Fiber-Reinforced Cemented Tailings Composites. *Int. J. Miner. Metall. Mater.* 29, 1. doi:10.1007/s12613-021-2351-x

Li, J., Huang, Y., Li, W., Guo, Y., Ouyang, S., and Cao, G. (2021). Study on Dynamic Adsorption Characteristics of Broken Coal Gangue to Heavy Metal Ions under Leaching Condition and its Cleaner Mechanism to Mine Water. *J. Clean. Prod.* 329, 129756. doi:10.1016/j.jclepro.2021.129756

Li, J., Huang, Y., Pu, H., Gao, H., Li, Y., Ouyang, S., et al. (2021). Influence of Block Shape on Macroscopic Deformation Response and Meso-Fabric Evolution of Crushed Gangue under the Triaxial Compression. *Powder Tech.* 384, 112–124. doi:10.1016/j.powtec.2021.02.001

Liu, L., Xin, J., Huan, C., Qi, C., Zhou, W., and Song, K.-I. (2020). Pore and Strength Characteristics of Cemented Paste Backfill Using Sulphide Tailings: Effect of sulphur Content. *Construction Building Mater.* 237, 117452. doi:10.1016/j.conbuildmat.2019.117452

Mashifana, T., and Sithole, T. (2021). Clean Production of Sustainable Backfill Material from Waste Gold Tailings and Slag. *J. Clean. Prod.* 308, 127357. doi:10.1016/j.jclepro.2021.127357

Mower, T. M., and Long, M. J. (2016). Mechanical Behavior of Additive Manufactured, Powder-Bed Laser-Fused Materials. *Mater. Sci. Eng. A* 651, 198–213. doi:10.1016/j.msea.2015.10.068

Ouellet, S., Bussière, B., Aubertin, M., and Benzaazoua, M. (2007). Microstructural Evolution of Cemented Paste Backfill: Mercury Intrusion Porosimetry Test Results. *Cement Concrete Res.* 37, 1654–1665. doi:10.1016/j.cemconres.2007.08.016

Qi, C. C., Ly, H. B., Le, L. M., Yang, X. Y., Guo, L., and Pham, B. T. (2021). Improved Strength Prediction of Cemented Paste Backfill Using a Novel Model Based on Adaptive Neuro Fuzzy Inference System and Artificial Bee colony. *Construction Building Mater.* 284, 122857. doi:10.1016/j.conbuildmat.2021.122857

Qiu, J. P., Guo, Z. B., Yang, L., Jiang, H. Q., and Zhao, Y. L. (2020). Effect of Tailings Fineness on Flow, Strength, Ultrasonic and Microstructure Characteristics of Cemented Paste Backfill. *Construction Building Mater.* 263, 120645. doi:10.1016/j.conbuildmat.2020.120645

Sharma, K., and Kumar, A. (2021). Influence of rice Husk Ash, Lime and Cement on Compaction and Strength Properties of Copper Slag. *Transp Geotech* 27, 100464. doi:10.1016/j.trgeo.2020.100464,

Sun, W., Zuo, Y., Wu, Z., Liu, H., Xi, S., Shui, Y., et al. (2019). Fractal Analysis of Pores and the Pore Structure of the Lower Cambrian Niutitang Shale in Northern Guizhou Province: Investigations Using NMR, SEM and Image Analyses. *Mar. Pet. Geology.* 99, 416–428. doi:10.1016/j.marpetgeo.2018.10.042

Tan, Y.-y., Yu, X., Elmo, D., Xu, L.-h., and Song, W.-d. (2019). Experimental Study on Dynamic Mechanical Property of Cemented Tailings Backfill under SHPB Impact Loading. *Int. J. Miner. Metall. Mater.* 26, 404–416. doi:10.1007/s12613-019-1749-1

Tana, A. E. B., Yin, S. H., and Wang, L. M. (2021). Investigation on Mechanical Characteristics and Microstructure of Cemented Whole Tailings Backfill. *Minerals* 11, 592. doi:10.3390/min11060592

Wang, H. C., Qi, T. Y., Feng, G. R., Wen, X. Z., Wang, Z. H., Shi, X. D., et al. (2021). Effect of Partial Substitution of Corn Straw Fly Ash for Fly Ash as Supplementary Cementitious Material on the Mechanical Properties of Cemented Coal Gangue Backfill. *Construction Building Mater.* 280, 122553. doi:10.1016/j.conbuildmat.2021.122553

Wang, J., Fu, J. X., and Song, W. D. (2020). Mechanical Properties and Microstructure of Layered Cemented Paste Backfill under Triaxial Cyclic Loading and Unloading. *Construction Building Mater.*, 257. 119540. doi:10.1016/j.conbuildmat.2020.119540

Wang, L., Liu, J.-f., Pei, J.-l., Xu, H.-n., and Bian, Y. (2015). Mechanical and Permeability Characteristics of Rock under Hydro-Mechanical Coupling Conditions. *Environ. Earth Sci.* 73, 5987–5996. doi:10.1007/s12665-015-4190-4

Wang, S., Song, X. P., Wei, M. L., Liu, W., Wang, X. J., Ke, Y. X., et al. (2021). Strength Characteristics and Microstructure Evolution of Cemented Tailings Backfill with rice Straw Ash as an Alternative Binder. *Construction Building Mater.* 297, 123780. doi:10.1016/j.conbuildmat.2021.123780

Wang, S., Song, X. P., Chen, Q. S., Wang, X. J., Wei, M. L., Ke, Y. X., et al. (2020). Mechanical Properties of Cemented Tailings Backfill Containing Alkalized rice Straw of Various Lengths. *J. Environ. Manage.* 276, 111124. doi:10.1016/j.jenvman.2020.111124

Wu, D., Sun, W., Liu, S., and Qu, C. L. (2021). Effect of Microwave Heating on Thermo-Mechanical Behavior of Cemented Tailings Backfill. *Construction Building Mater.* 266, 121180. doi:10.1016/j.conbuildmat.2020.121180

Wu, Y., Tahmasebi, P., Lin, C., Zahid, M. A., Dong, C., Golab, A. N., et al. (2019). A Comprehensive Study on Geometric, Topological and Fractal Characterizations of Pore Systems in Low-Permeability Reservoirs Based on SEM, MICP, NMR, and X-ray CT Experiments. *Mar. Pet. Geology.* 103, 12–28. doi:10.1016/j.marpetgeo.2019.02.003

Xiao, W. J., Zhang, D. M., and Wang, X. J. (2020). Experimental Study on Progressive Failure Process and Permeability Characteristics of Red sandstone under Seepage Pressure. *Eng. Geol.* 265, 105406. doi:10.1016/j.enggeo.2019.105406

Xiu, Z. G., Wang, S. H., Ji, Y. C., Wang, F. L., Ren, F. Y., and Nguyen, V. T. (2021). Loading Rate Effect on the Uniaxial Compressive Strength (UCS) Behavior of Cemented Paste Backfill (CPB). *Construction Building Mater.* 271, 121526. doi:10.1016/j.conbuildmat.2020.121526

Xu, W. B., Li, Q. L., and Liu, B. (2020). Coupled Effect of Curing Temperature and Age on Compressive Behavior, Microstructure and Ultrasonic Properties of Cemented Tailings Backfill. *Construction Building Mater.* 237, 117738. doi:10.1016/j.conbuildmat.2019.117738

Xu, W., Cao, Y., and Liu, B. (2019). Strength Efficiency Evaluation of Cemented Tailings Backfill with Different Stratified Structures. *Eng. Structures* 180, 18–28. doi:10.1016/j.engstruct.2018.11.030

Yang, L. H., Wang, H. J., Li, H., and Zhou, X. (2019). Effect of High Mixing Intensity on Rheological Properties of Cemented Paste Backfill. *Minerals* 9, 240. doi:10.3390/min9040240

Yilmaz, E., Belem, T., and Benzaazoua, M. (2015). Specimen Size Effect on Strength Behavior of Cemented Paste Backfills Subjected to Different Placement Conditions. *Eng. Geology.* 185, 52–62. doi:10.1016/j.enggeo.2014.11.015

Yilmaz, E., Benzaazoua, M., Belem, T., and Bussière, B. (2009). Effect of Curing under Pressure on Compressive Strength Development of Cemented Paste Backfill. *Minerals Eng.* 22, 772–785. doi:10.1016/j.mineng.2009.02.002

Yin, S. H., Shao, Y. J., Wu, A. X., Wang, Z. Y., and Yang, L. H. (2020). Assessment of Expansion and Strength Properties of Sulfidic Cemented Paste Backfill Cored from Deep Underground Stopes. *Construction Building Mater.* 230, 116983. doi:10.1016/j.conbuildmat.2019.116983

Yu, S., Ke, Y., Deng, H., Tian, G., and Deng, J. (2021). Experimental Investigation of Porous and Mechanical Characteristics of Single-Crack Rock-like Material under Freeze-Thaw Weathering. *Minerals* 11, 1318. doi:10.3390/min11121318

Zhang, J. Z., Tang, Y. J., He, D. X., Sun, P., and Zou, X. Y. (2020). Full-scale Nanopore System and Fractal Characteristics of clay-rich Lacustrine Shale Combining FE-SEM, nano-CT, Gas Adsorption and Mercury Intrusion Porosimetry. *Appl. Clay Sci.* 196, 105758. doi:10.1016/j.clay.2020.105758

Zhao, Y., Wang, C. L., Ning, L., Zhao, H. F., and Bi, J. (2022). Pore and Fracture Development in Coal under Stress Conditions Based on Nuclear Magnetic Resonance and Fractal Theory. *Fuel* 309, 122112. doi:10.1016/j.fuel.2021.122112

Zheng, J., Zhu, Y., and Zhao, Z. (2016). Utilization of limestone Powder and Water-Reducing Admixture in Cemented Paste Backfill of Coarse Copper Mine Tailings. *Construction Building Mater.* 124, 31–36. doi:10.1016/j.conbuildmat.2016.07.055

Zhou, N., Du, E. B., Zhang, J. X., Zhu, C. L., and Zhou, H. Q. (2021). Mechanical Properties Improvement of Sand-Based Cemented Backfill Body by Adding Glass Fibers of Different Lengths and Ratios. *Construction Building Mater.* 280, 122408. doi:10.1016/j.conbuildmat.2021.122408

Zhou, N., Ma, H. B., Ouyang, S. Y., Germain, D., and Hou, T. (2019). Influential Factors in Transportation and Mechanical Properties of Aeolian Sand-Based Cemented Filling Material. *Minerals* 9, 116. doi:10.3390/min9020116

Conflict of Interest: The authors declare that the research was conducted in the absence of any commercial or financial relationships that could be construed as a potential conflict of interest.

Publisher's Note: All claims expressed in this article are solely those of the authors and do not necessarily represent those of their affiliated organizations, or those of the publisher, the editors and the reviewers. Any product that may be evaluated in this article, or claim that may be made by its manufacturer, is not guaranteed or endorsed by the publisher.